High Detectivity of Metal–Semiconductor–Metal Ga_2O_3 Solar-Blind Photodetector Through Thickness-Regulated Gain

Zhiyao Zheng, Baoshi Qiao, Zhenzhong Zhang, Xiaoqian Huang, Xiuhua Xie, Binghui Li, Xing Chen, Kewei Liu, Lei Liu, and Dezhen Shen, *Member, IEEE*

***Abstract*— Detectivity is the most key parameter in weak-signal photodetection, which depends on high photoresponse and low noise simultaneously. In this work, metal–semiconductor–metal solar-blind UV detectors with internal gain were fabricated based on high resistant and a certain oxygen vacancy density Ga_2O_3 thin films. Electrical measurements and electric field simulation indicated that thickening the active layer is helpful for high responsivity. The gain is dominated by the tunneling effect in high electric field under the electrodes. A high photoresponse of 371 A/W and a normalized detectivity up to 6.6 $\times$ 10^{16} Jones were obtained.**

***Index Terms*— High detectivity, solar-blind photodetectors, thickness-regulated.**

I. Introduction

BENEFITING from ultralow background noise disturbing, solar-blind ultraviolet photodetector shows great potential in many occasions, such as fire alarming, missile warning, secret communication, and ozone detection [1]–[3]. Among all the applications, the detection to weak signal commonly plays an important role, which is usually evaluated by the specific detectivity. It depends on high photoresponse and low noise simultaneously [4], [5]. Compared with silicon, which is widely used in commercialized solar-blind photodetector, wide bandgap materials, such as AlGaN, MgZnO, Ga_2O_3, and diamond, attract more and more interests for their intrinsic spectral selectivity and much lower dark noise [6]–[8]. Among these materials, β-Ga_2O_3 is gradually becoming an essential part in solar-blind photodetection materials, due to its fixed composition, intrinsic solar-blind bandgap, economical preparation method, and adaptability to bad working environment [9]–[13].

Undoped β-Ga_2O_3 usually shows high resistivity, which is beneficial to decrease the dark current for photodetection [14], [15]. However, the devices based on such high resistant β-Ga_2O_3 often showed poor responsivity when no gain was introduced [16]–[18]. In our early work, an internal gain was observed in Ga_2O_3-based metal–semiconductor–metal (MSM) photodetector [19]. An extremely unbalanced resistance distribution between the exposed and sheltered part leads to an ultrahigh electric field under the electrodes in device. A detectivity near 10^{16} Jones was obtained. Based on the same structured photodetector, Li *et al.* [20] also achieved a detectivity up to 2 $\times$ 10^{16} Jones.

In this work, we grew β-Ga_2O_3 thin films at different oxygen pressures and fabricated MSM photodetectors. It was found that thickening the active layer is helpful for increasing the electric field under electrodes and the detectivity subsequently. An ultrahigh rejection ratio at 254/365 nm of 10^8 was observed. The device showed a normalized detectivity up to 6.6 $\times$ 10^{16} Jones and fast response with a decay time of 1.3 μs. The gain is dominated by tunneling effect assisted by oxygen vacancy (V_O).

II. Experiment

β-Ga_2O_3 thin films were grown on c-plane sapphire by metalorganic chemical vapor deposition (MOCVD). The precleaning process was carried out with ultrasonic bathing in trichloroethylene, acetone, ethyl alcohol, and deionized water. The growth temperature and pressure were kept at 700 °C and 650 Pa, respectively. Triethylgallium was used as the precursors with the flow rates of 4 SCCM (blowing out from the cylinder at 10 °C). The 120 and 1000 SCCM of 5-N O_2 were adopted to growth the Ga_2O_3 thin films with different V_O densities. The thickness of the thin film was regulated from 200 to 400 nm by changing growth time

Manuscript received 2 June 2022; accepted 15 June 2022. Date of publication 23 June 2022; date of current version 25 July 2022. This work was supported in part by the National Natural Science Foundation of China under Grant 11727902, Grant 62074146, Grant 11804335, Grant 61875194, Grant 61975204, Grant 11974344, Grant 62074148, and Grant 12074372; in part by the 100 Talents Program of the Chinese Academy of Sciences; in part by the Fund from Jilin Province under Grant 20190103042JH. The review of this article was arranged by Editor H. Nguyen. *(Corresponding author: Zhenzhong Zhang.)*

Zhiyao Zheng is with the Changchun Institute of Optics, Fine Mechanics and Physics, Chinese Academy of Sciences, Changchun 130033, China, and also with the Center of Materials Science and Optoelectronics Engineering, University of the Chinese Academy of Sciences, Beijing 100049, China.

Baoshi Qiao, Xiaoqian Huang, Xiuhua Xie, Binghui Li, Xing Chen, Kewei Liu, Lei Liu, and Dezhen Shen are with the Changchun Institute of Optics, Fine Mechanics and Physics, Chinese Academy of Sciences, Changchun 130033, China.

Zhenzhong Zhang is with Dalian University of Technology, Dalian, Liaoning 116024, China (e-mail: zhangzz@dlut.edu.cn).

Color versions of one or more figures in this article are available at https://doi.org/10.1109/TED.2022.3184277.

Digital Object Identifier 10.1109/TED.2022.3184277

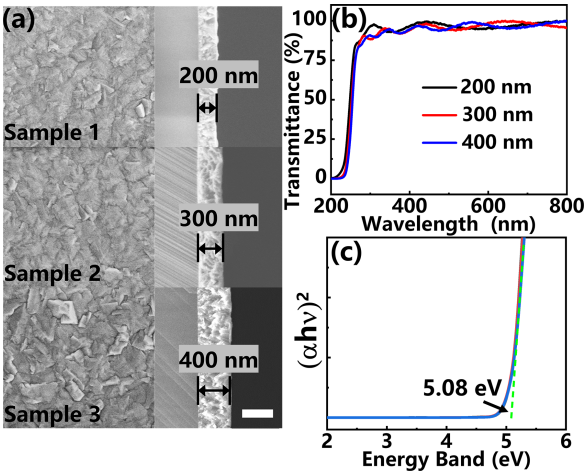

Fig. 1. (a) SEM images of thin films with different growth times. Scale bar: 400 nm. (b) Optical transmission spectrum of the β-Ga_2O_3 films. (c) Optical bandgap fitting from transmission spectrum.

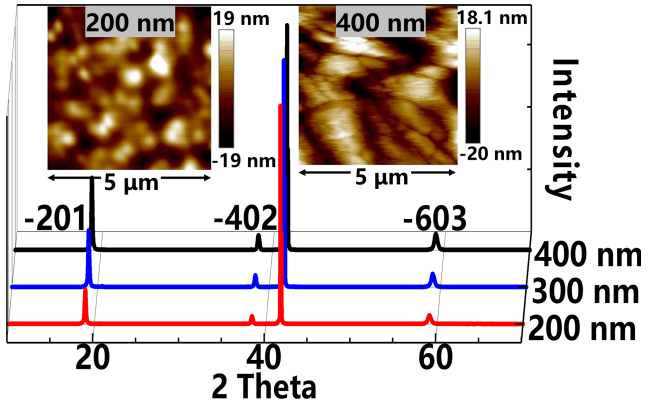

Fig. 2. XRD spectra of β-Ga_2O_3 thin films with different thicknesses. The insets show the transformation of surface morphology.

from 2 to 4 h. Post-thermal annealing was carried out in air atmosphere for 30 min at 800 °C to improve further the crystal quality. This annealing process is demonstrated to reduce the conductivity by more than three orders of magnitude [19]. The MSM structured device was fabricated by lithography and the following sputtering gold electrodes. The interdigital electrodes consist of 25 pairs of Au fingers with 10-μm width and 10-μm interval.

Scanning electron microscopy (SEM) (HITACHI S-4800) and X-ray diffraction (XRD) (Bruker D8GADDS) with Cu Kα radiation ($\lambda = 0.154$ nm) were used to characterize the morphology and structure, respectively. Surface morphology was characterized by atomic force microscope (AFM) (BRUKER MULTIMODE 8). Transmittance spectra were measured on the Shimadzu UV-3101PC spectrophotometer. The I–V and I–t curves were obtained on a semiconductor device analyzer (Agilent B1500A). The photoresponse spectra were measured through responsivity measurement system equipped with an SR 830 lock-in amplifier and 150-W Xe lamp. Time-resolved response was recorded by a Tektronics DPO5104 oscilloscope with 110-Ω load resistance under the excitation of 254-nm laser with 10-ns pulsewidth.

III. Results and Discussion

Fig. 1(a) shows the SEM images of the β-Ga_2O_3 thin films. As can be seen from the surface images, the thin films are composed of dense grains. By the cross-sectional graphics, it is found that the thin films show good thickness uniformity, and the thickness increases from 200 to 400 nm as the growth time changes from 2 to 4 h. Fig. 1(b) shows the transmission spectra of Ga_2O_3 samples. All the samples show sharp adsorption edge, indicating their good optical quality. All the samples show almost the same bandgap value of 5.08 eV according to the $(\alpha h\nu)^2 \sim h\nu$ curve [21], indicating the uniformity in optical quality among these samples, as shown in Fig. 1(c). Fig. 2 shows the XRD spectra of thin films with different thicknesses. All the samples show the single orientation of (−201). The full-width at half-maximum (FWHM) of peak (−201) is 0.188°, 0.173°, and 0.175° for the films with the thickness of 200, 300, and 400 nm, respectively. Small FWHM indicates the high crystal quality of Ga_2O_3 thin film. The surface morphology of annealed Ga_2O_3 thin film was characterized by AFM, as shown in the inset. It is found that the samples with 200 and 400 nm thickness show similar roughness 6.92 and 8.14 nm, respectively. According to previous reports, such difference in roughness almost brought no difference in photodetection performance [22], [23].

To investigate the UV response properties of the Ga_2O_3 thin film, MSM structured devices were fabricated by the liftoff process of photolithography. The pattern covers a region (effective area) of 0.5 mm × 1.0 mm. The I–V curves of the three samples under dark, 365-nm illumination, and 254-nm illumination are shown in Fig. 3(a)–(c), respectively. The dark I–V curves are almost linear, indicating approximate ohmic contact. It indicates that the Femi level of Au is higher than the one of insulating Ga_2O_3 in this work. Under 365-nm illumination (850 μW/cm^2), the current shows a certain increase, and the I–V curve keeps semilinear shape. For the thickest sample, the currents at 20 V in dark and under 365-nm illumination are 514 fA and 12.5 pA, respectively. Under 254-nm illumination (890 μW/cm^2), the photocurrent at 20-V bias is 1578 μA. Thus, the photo-to-dark current ratio (PDCR) and rejection ratio at 254/365 nm can reach 3.2×10^9 and 1.1×10^8, respectively.

According to the 254-nm illumination density, photocurrent, dark current, and effective area [24]–[26], the responsivities of three samples are calculated to be 6.2, 94, and 371 A/W, and the corresponding external quantum efficiencies (EQE) are 3028%, 45 900%, and 181 355%, respectively. Due to ultralow dark current and high responsivity, the highest specific detectivity reaches 6.6×10^{16} Jones [27], which is larger than most reported values. Besides that, to show the spectral selectivity, Fig. 3(d) shows the response spectra. It could be found that all the devices show satisfying solar-blind selectivity and increasing peak responsivity with thickness. The lower responsivity than that obtained from the I–V measurement is due to the lower illumination density, which will be discussed later.

The increase of responsivity partly originates from the increase in light absorption. From Fig. 1(b), the transmittance ratio at 254 nm is estimated to be 0.69, 0.55, and 0.47 for

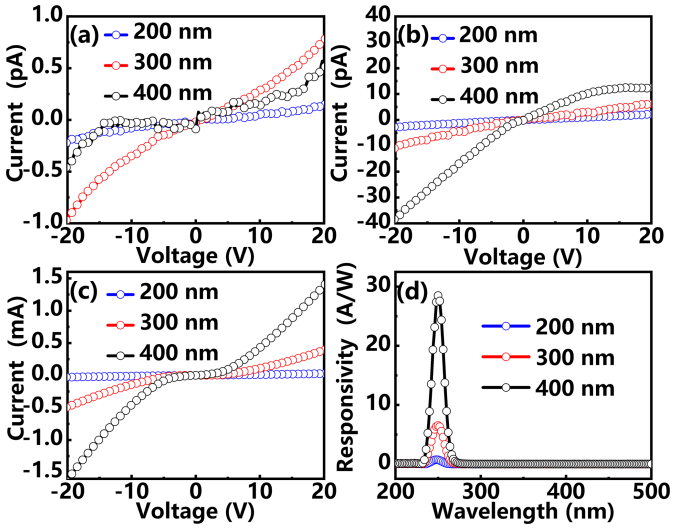

Fig. 3. *I–V* curves of samples with 200, 300, and 400 nm thickness under (a) dark, (b) 365-nm illumination, and (c) 254-nm illumination. (d) Response spectra.

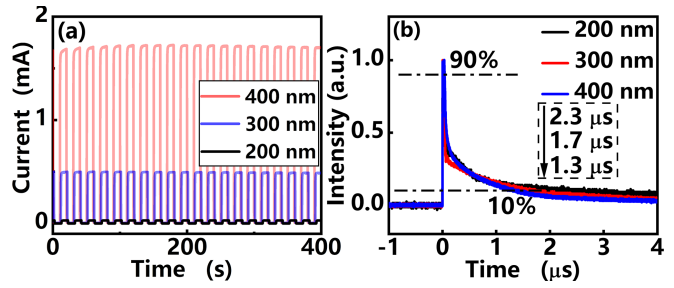

Fig. 4. (a) *I–t* curves with turning on/off the 254-nm illumination of different thickness devices. (b) Response speed of different thickness devices under 10-ns 254-nm pulse laser.

the thin film with the thickness of 200, 300, and 400 nm, respectively. However, this little variation cannot bring such large increase in the responsivity and EQE. It indicates that there are some gains amplifying the current with thickening the active layer, i.e., photoconductive gain, avalanche gain, or tunneling. Fig. 4(a) shows the *I–t* curves at 20-V bias of the three samples with switching 254-nm illumination. The device exhibits highly stable and relatively high speed. Noting that there is a climb after the sharp rising edge, which is the characteristic of the defect associated photoconductive gain. However, this photoconductive gain is far from the main part of the total gain because the climb range is too small for the total photocurrent, and persistent photocurrent is not observed clearly in the decay edge. Fig. 4(b) shows the accurate time-response results collected by an oscilloscope with 110-Ω load resistance, which is far smaller than the resistance of the device under illumination. The decay times are 2.3, 1.7, and 1.3 μs of the three samples. If the gain is completely caused by photoconduction, the EQE value is calculated to be about only 10 000% according to the carrier mobility value [19] and decay time as the lifetime of minor carrier, which is far less than the EQE obtained from 371 A/W. Therefore, photoconductive gain is not the main cause for the large responsivity.

Avalanche gain or tunneling can support high EQE and fast response simultaneously. Because both the two effects are

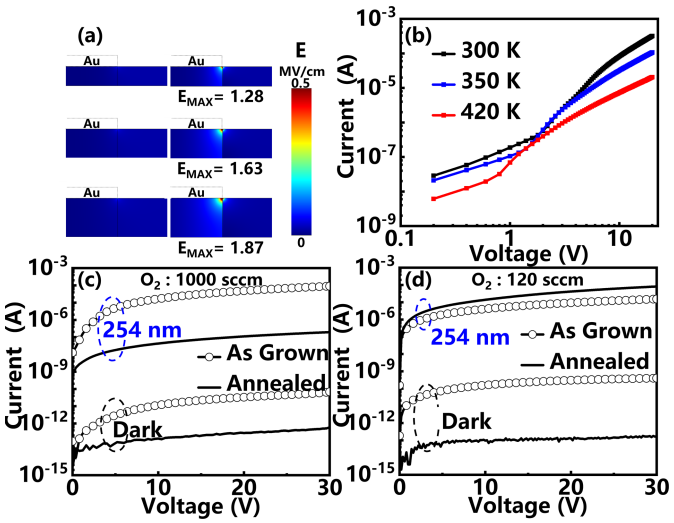

Fig. 5. (a) Simulated distribution of electric field in the device with 200, 300, and 400 nm-thickness samples in dark (left) and under 254-nm illumination (right). (b) *I–V* curves under 254-nm illumination at different temperatures. The *I–V* curves of (c) low and (d) high V_O density Ga_2O_3 device before and after annealing.

strongly associated with electric field, it is necessary to discuss the electric field distribution in the thin film. Undoubtedly, the thickness of Ga_2O_3 is the main factor, which affects the distribution of electric field. It can be deduced that a thicker Ga_2O_3 can absorb more UV illumination and reduce the series resistance. In consequence, the electric field under electrodes will increase. Fig. 5(a) shows the simulation of electric field performed by COMSOL. All the simulation parameters were obtained based on experimental data. Gold was selected as the electrode material. Due to the linear dark current in the MSM device, the contact was defined to be ohmic. The width of electrode and interval was both set as 10 μm. The conductivity of the covered region was set as 5×10^{-10} S/m according to *I–V* measurement in dark. In the exposed region, it was set according to the *I–V* measurements under illumination. For the simulation in dark, the electric field almost distributes uniformly. Under illumination, the electric field concentrates near the edge of electrode, and the intensity increases quickly with thickening the film. These simulation results are in accordance with the experimental phenomenon that this gain exists only under 254-nm illumination and could increase with thickening the active layer. A higher responsivity can be reached with thicker film. It is obvious that the larger the 254-nm illumination density is, the more unevenly the electric field distributes. This is why the responsivity in Fig. 3(d) is smaller than the one calculated in Fig. 3(a).

The *I–V* curves at different temperatures were commonly adopted to distinguish the gain type. As shown in Fig. 5(b), the inflection point of photocurrent shifts to lower voltage with increasing the temperature. Also, such low inflection point voltage has not been observed in the MSM structured device based on wide bandgap materials. It indicates that the large responsivity is dominated by some kind of tunneling gain in high electric field under electrodes, not avalanche. According to the simulation, the electric field under electrode is markedly lower than the breakdown electric field

of β-Ga_2O_3 (8 MV/cm). Therefore, the tunneling should not occur directly between the valence band and the conduction band, but with the help of some defects with energy levels in bandgap.

We grew β-Ga_2O_3 thin films at different oxygen pressures, which were expected to have different V_O and Ga interstitial densities. As shown in Fig. 5(c) and (d), the I–V curves of thin film grown with high and low oxygen pressure exhibit marked differences. For the sample grown with high oxygen pressure, the photocurrent and dark current show a similar decrease after thermal annealing, which keeps a certain photo-to-dark ratio. The decrease of dark current and photocurrent is caused by the repair of shallow donors, such as Ga interstitial. For the sample grown with low oxygen pressure, the thermal annealing decreases the dark current by about three orders of magnitude, which is also caused by the repair of shallow donors. However, the photocurrent keeps its high level after the thermal annealing. It means that some defects remain after annealing. Some deep-level defects, such as V_O with different charge states, can play the bridge for tunneling between the valence band and the conduction band. These deep-level defects are responsible for the large gain of the detector with low dark current.

IV. Conclusion

In summary, we grew β-Ga_2O_3 thin films at different oxygen pressures by the MOCVD method and fabricated MSM photodetectors. It was found that thickening the active layer is helpful for increasing the electric field under electrodes and the detectivity subsequently. This device shows a rejection ratio at 254/365 nm of 1.1×10^8, an excellent fast response speed with a 90%–10% decay time of 1.3 μs as well. A photoresponsivity of 371 A/W and a specific detectivity of up to 6.6×10^{16} Jones were obtained. The light-induced gain was demonstrated to be dominated by the tunneling effect. Some deep-level defects, such as V_O with different charge states, can play the bridge for tunneling between the valence band and the conduction band.

References

[1] H. Chen *et al.*, "Ultrasensitive self-powered solar-blind deep-ultraviolet photodetector based on all-solid-state polyaniline/MgZnO bilayer," *Small*, vol. 12, no. 42, pp. 5809–5816, Nov. 2016, doi: 10.1002/smll.201601913.

[2] Y. An *et al.*, "Au plasmon enhanced high performance β-Ga_2O_3 solar-blind photo-detector," *Prog. Natural Sci., Mater. Int.*, vol. 26, no. 1, pp. 65–68, Feb. 2016, doi: 10.1016/j.pnsc.2016.01.008.

[3] Y. Xu, X. Chen, Y. Zhang, F. Ren, S. Gu, and J. Ye, "Fast speed Ga_2O_3 solar-blind Schottky photodiodes with large sensitive area," *IEEE Electron Device Lett.*, vol. 41, no. 7, pp. 997–1000, Jul. 2020, doi: 10.1109/LED.2020.2998804.

[4] L. Zhang *et al.*, "Solar-blind ultraviolet photodetector based on vertically aligned single-crystalline β-Ga_2O_3 nanowire arrays," *Nanophotonics*, vol. 9, no. 15, pp. 4497–4503, Oct. 2020, doi: 10.1515/nanoph-2020-0295.

[5] J. Ding, S. Du, Z. Zuo, Y. Zhao, H. Cui, and X. Zhan, "High detectivity and rapid response in perovskite $CsPbBr_3$ single-crystal photodetector," *J. Phys. Chem. C*, vol. 121, no. 9, pp. 4917–4923, Mar. 2017, doi: 10.1021/acs.jpcc.7b01171.

[6] Z. Wang, X. Chen, F.-F. Ren, S. Gu, and J. Ye, "Deep-level defects in gallium oxide," *J. Phys. D, Appl. Phys.*, vol. 54, no. 4, Nov. 2020, Art. no. 043002, doi: 10.1088/1361-6463/abbeb1.

[7] F. H. Teherani *et al.*, "MgZnO grown by molecular beam epitaxy on n-type β-Ga_2O_3 for UV Schottky barrier solar-blind photodetectors," *Proc. SPIE*, vol. 10105, Feb. 2017, Art. no. 101051N, doi: 10.1117/12.2254937.

[8] N. Liu *et al.*, "Fast-response amorphous Ga_2O_3 solar-blind ultraviolet photodetectors tuned by a polar AlN template," *IEEE Electron Device Lett.*, vol. 43, no. 1, pp. 68–71, Jan. 2022, doi: 10.1109/LED.2021.3132497.

[9] Z. Liu *et al.*, "Construction of a β-Ga_2O_3-based metal–oxide–semiconductor-structured photodiode for high-performance dual-mode solar-blind detector applications," *J. Mater. Chem. C*, vol. 8, no. 15, pp. 5071–5081, Apr. 2020, doi: 10.1039/d0tc00100g.

[10] S. Kim and J. Kim, "Highly selective ozone-treated β-Ga_2O_3 solar-blind deep-UV photodetectors," *Appl. Phys. Lett.*, vol. 117, no. 26, Dec. 2020, Art. no. 261101, doi: 10.1063/5.0030400.

[11] C. Chen *et al.*, "High-performance β-Ga_2O_3 solar-blind photodetector with extremely low working voltage," *IEEE Electron Device Lett.*, vol. 42, no. 10, pp. 1492–1495, Oct. 2021, doi: 10.1109/LED.2021.3108190.

[12] E. Ahmadi *et al.*, "Ge doping of β-Ga_2O_3 films grown by plasma-assisted molecular beam epitaxy," *Appl. Phys. Exp.*, vol. 10, no. 4, Apr. 2017, Art. no. 041102, doi: 10.7567/apex.10.041102.

[13] Y.-C. Chen *et al.*, "Self-powered diamond/β-Ga_2O_3 photodetectors for solar-blind imaging," *J. Mater. Chem. C*, vol. 6, no. 21, pp. 5727–5732, 2018, doi: 10.1039/c8tc01122b.

[14] A. Mauze, Y. Zhang, T. Itoh, E. Ahmadi, and J. S. Speck, "Sn doping of (010) β-Ga_2O_3 films grown by plasma-assisted molecular beam epitaxy," *Appl. Phys. Lett.*, vol. 117, no. 22, Nov. 2020, Art. no. 222102, doi: 10.1063/5.0027870.

[15] X. Du *et al.*, "Preparation and characterization of Sn-doped β-Ga_2O_3 homoepitaxial films by MOCVD," *J. Mater. Sci.*, vol. 50, no. 8, pp. 3252–3257, Apr. 2015, doi: 10.1007/s10853-015-8893-4.

[16] C. Zhou *et al.*, "Performance improvement of amorphous Ga_2O_3 ultraviolet photodetector by annealing under oxygen atmosphere," *J. Alloys Compounds*, vol. 840, Nov. 2020, Art. no. 155585, doi: 10.1016/j.jallcom.2020.155585.

[17] S. Cui, Z. Mei, Y. Zhang, H. Liang, and X. Du, "Room-temperature fabricated amorphous Ga_2O_3 high-response-speed solar-blind photodetector on rigid and flexible substrates," *Adv. Opt. Mater.*, vol. 5, no. 19, Oct. 2017, Art. no. 1700454, doi: 10.1002/adom.201700454.

[18] G. C. Hu, C. X. Shan, N. Zhang, M. M. Jiang, S. P. Wang, and D. Z. Shen, "High gain Ga_2O_3 solar-blind photodetectors realized via a carrier multiplication process," *Opt. Exp.*, vol. 23, no. 10, pp. 13554–13561, May 2015, doi: 10.1364/OE.23.013554.

[19] B. Qiao *et al.*, "Avalanche gain in metal–semiconductor–metal Ga_2O_3 solar-blind photodiodes," *J. Phys. Chem. C*, vol. 123, no. 30, pp. 18516–18520, Aug. 2019, doi: 10.1021/acs.jpcc.9b02608.

[20] Z. Li *et al.*, "High-performance β-Ga_2O_3 solar-blind Schottky barrier photodiode with record detectivity and ultrahigh gain via carrier multiplication process," *IEEE Electron Device Lett.*, vol. 41, no. 12, pp. 1794–1797, Dec. 2020, doi: 10.1109/LED.2020.3032290.

[21] Q. Liu *et al.*, "Stabilizing the metastable γ phase in Ga_2O_3 thin films by Cu doping," *J. Alloys Compounds*, vol. 731, pp. 1225–1229, Jan. 2018, doi: 10.1016/j.jallcom.2017.10.162.

[22] L. Huang *et al.*, "Comparison study of β-Ga_2O_3 photodetectors grown on sapphire at different oxygen pressures," *IEEE Photon. J.*, vol. 9, no. 4, pp. 1–8, Aug. 2017, doi: 10.1109/JPHOT.2017.2731625.

[23] N. Blumenschein, T. Paskova, and J. F. Muth, "Effect of growth pressure on PLD-deposited gallium oxide thin films for deep-UV photodetectors," *Phys. Status Solidi (A)*, vol. 216, no. 20, Oct. 2019, Art. no. 1900098, doi: 10.1002/pssa.201900098.

[24] C. Xie, P. You, Z. Liu, L. Li, and F. Yan, "Ultrasensitive broadband phototransistors based on perovskite/organic-semiconductor vertical heterojunctions," *Light, Sci. Appl.*, vol. 6, no. 8, Aug. 2017, Art. no. e17023, doi: 10.1038/lsa.2017.23.

[25] X. Shen, L. Duan, J. Li, X. Zhang, X. Li, and W. Lü, "Enhanced performance of flexible ultraviolet photodetectors based on carbon nitride quantum dot/ZnO nanowire nanocomposites," *Mater. Res. Exp.*, vol. 6, no. 4, Jan. 2019, Art. no. 045002, doi: 10.1088/2053-1591/aaf915.

[26] S. Oh, C.-K. Kim, and J. Kim, "High responsivity β-Ga_2O_3 metal–semiconductor–metal solar-blind photodetectors with ultraviolet transparent graphene electrodes," *ACS Photon.*, vol. 5, no. 3, pp. 1123–1128, Mar. 2018, doi: 10.1021/acsphotonics.7b01486.

[27] Y. Wang *et al.*, "A high responsivity self-powered solar-blind DUV photodetector based on a nitrogen-doped graphene/β-Ga_2O_3 microwire p-n heterojunction," *IEEE Electron Device Lett.*, early access, May 4, 2022, doi: 10.1109/LED.2022.3172728.